Astron. Astrophys. 323, 189–201 (1997)

ASTRONOMY
AND
ASTROPHYSICS

Ionization structure of the shells surrounding Herbig Ae/Be stars

A.F. Kholtygin[1], **V.B. Il'in**[1,2], **and N.V. Voshchinnikov**[1]

[1] Astronomical Institute, St. Petersburg University, St. Petersburg, 198904 Russia
[2] Max Planck Society, Research Unit "Dust in Star-Forming Regions", Schillergäßchen 3, D-07745 Jena, Germany

Received 6 October 1996 / Accepted 19 December 1996

Abstract. The ionization balance of the circumstellar gas around Herbig Ae/Be stars is studied. The model used is based on the results obtained by Catala & Kunasz (1987) for the wind formation region of the typical Herbig Ae/Be star AB Aur. Large brightness variations of some stars are assumed to be due to their obscuration by clumps in the shells, and the gas ionization in the clumps is also considered.

It is shown that the source of ionization of gas is the radiation of the stellar photosphere and chromosphere, and the main processes that determine the ionization structure of the shells are photoionization, photorecombination and dielectronic recombination. The column density of Na I and Ca II, the central optical thickness and the equivalent width of the circumstellar Ca II K and Na I D_2 absorption lines are estimated and their dependence on the model parameters is examined. It is found that the clumps are the places where sufficiently strong variable lines may originate. The equivalent width of the lines are mainly determined by the gas to dust ratio and the element depletion in the clumps. The lines could be observed with the current large telescopes and give information on the nature of the clumps being probably the places of planet formation. The model is used to interpret two episodes of the spectral line variations observed for AB Aur and HR 5999.

Key words: circumstellar matter – stars: pre-main sequence – stars: individual: AB Aur, HR 5999 – line: formation

1. Introduction

Herbig Ae/Be (HAeBe) stars are young objects with large infrared excesses, variable brightness, intrinsic polarization and complex profiles of spectral lines. Almost all of these features are due to the presence of circumstellar shells. Such shells may be the precursors of the protoplanetary disks discovered around β Pictoris, Vega and other ordinary A-type stars.

Sporadic deep minima when the star fades down to 3 stellar magnitudes are the attributes of about 25% of HAeBe stars (Thé et al. 1994). Wenzel (1969) and Wenzel et al. (1971) first proposed that such minima could be produced by opaque circumstellar dust clouds or clumps moving between the star and observer. The model of variable circumstellar extinction has been extended by Grinin (1988) and Voshchinnikov & Grinin (1992) to explain the behaviour of both colour excesses (the blueing effect) and linear polarization in minima. These effects were related with the light scattering by small grains distributed in the shells.

Extensive spectral observations of HAeBe stars have been made in the visual, near infrared and ultraviolet regions, but detailed data have been obtained only for a few brightest stars: AB Aur, HR 5999, etc. (Praderie et al. 1982; Catala et al. 1986a, 1986b, 1993; Tjin A Djie et al. 1989; Blondel et al. 1989). The main feature in their spectra is the strong H_α line with a variable profile. The profiles of other lines are usually variable as well. A sophisticated model of the stellar chromosphere and the wind formation region of AB Aur has been developed by Catala et al. (1984) and Catala & Kunasz (1987, hereafter CK). It was based on the observations of H_α, C IV and Mg II lines originating in the *inner* layers of the circumstellar shells.

There are also observational data on the weak absorption lines which should originate in the *outer* layers of the shells (see, e.g., Tjin A Djie et al. 1989). As far as we know a simplified model of these layers has been created by Dyck & Milkey (1972) and only recently Sorelli et al. (1996) have studied the line formation in very small and dense clumps at the distances less than about 10 $R_\star$. The goal of the latter paper was to explain the redshifted absorption components of sodium lines.

In this paper, we consider the ionization degree of atoms in the outer layers of the shells and inside the clumps at the distances from the stars larger than the boundary of the H II region. Our model is based on the semi-empirical model of the wind formation region suggested by CK and the results of Voshchinnikov & Grinin (1992) obtained from the interpretation of the photometric and polarimetric observations of WW Vul in two minima. The aim of the work is to determinate whether the absorption lines originating in the clumps may be observed and what information could such observations provide. Observational data available are briefly discussed in Sect. 2. The model is described in Sect. 3. In Sect. 4, we present and discuss the results. The conclusions are summarized in Sect. 5. The expressions used in our calculations of the ionization and recombina-

Send offprint requests to: N.V. Voshchinnikov

tion rates, equivalent width of spectral lines, etc. are given in Appendices.

2. Summary of observational data

The variable absorption lines of Na I, Ca II, K I, Fe II, Mg II and other ions have been observed many times in the spectra of HAeBe stars (see, e.g., Finkenzeller & Mundt 1984; Catala et al. 1986a; Tjin A Djie et al. 1989 and for a recent review Catala 1994). Because of their variability, the lines can be considered as the circumstellar ones that originate in the layers located far from the stellar surface.

The lines are not very deep ($F/F_c \gtrsim 0.5$) and are saturated practically in all cases. The strengths of the sodium and calcium absorption lines are approximately equal (Catala et al. 1986a) and their equivalent width usually does not exceed 0.6 – 0.8 Å. However, the equivalent width of the Ca II H and K lines in the spectrum of HR 5999 reaches $W \approx 2$ – 3 Å (Tjin A Djie et al. 1989). These lines may be partially attributed to the stellar photosphere (Catala et al. 1986b).

The possibility to measure the line width (FWHM) is tightly connected with the spectral resolution used. For the narrow components of the Na I D and Ca II K lines, Catala et al. (1986a) found FWHM ≈ 10 – 20 km s^{-1}. Sometimes separated blueshifted or (and) redshifted components with the radial velocities up to 100 – 200 km s^{-1} are observed. The timescale of the absorption feature variations is about some hours or days and is often determined by the time resolution of observations.

Spectra of a few HAeBe stars have been obtained in deep minima: WW Vul by Timoshenko & Filip'ev (1983), SV Cep by Timoshenko (1985), HR 5999 by Tjin A Djie et al. (1989), and UX Ori by Grinin et al. (1994). Using the observations with a low spectral resolution Timoshenko & Filip'ev (1983) have detected the variations of W(Ca II) in the range ~ 1.5 – 3 Å for WW Vul. The authors described the quantitative behaviour of the line profiles as follows: when the star became brighter, the line became deeper and broader. The observations of HR 5999 by Tjin A Djie et al. (1989) appear to support this conclusion. Two spectra of UX Ori in a deep light minimum published by Grinin et al. (1994) show that the Na I D lines have weak inverse P Cyg profiles.

At present, it is difficult to find a definite relation between the behaviour of the absorption lines and the brightness variations. This was demonstrated by the figures in the papers of Grinin et al. (1994, 1996) and de Winter (1996). These figures show that the variations of profiles of the sodium lines are unrelated to the brightness variations. On the other hand, the detailed investigation of HR 5999 made by Tjin A Djie et al. (1989) shows that the equivalent width of the Na I D_2 line decreases from ~ 0.8 Å to ~ 0.2 Å when the star brightness changes from $6\overset{\mathrm{m}}{.}9$ to $7\overset{\mathrm{m}}{.}2$. The radial velocity of the line does not correlate with the brightness variations.

3. Model

For simplicity, the distribution of the gas and dust in the shell is assumed to depend only on the distance from the star. To explain of the brightness variations, we accept the variable circumstellar extinction model.

3.1. Structure of shell

The shell can be divided into the following regions: stellar chromosphere, H II, C II, and C I regions.

The radius of the H II region ($R_{\rm HII}$) should not be much larger than several AU. Otherwise, steady emission in the Balmer lines — the indicator of the H II regions would be observed. It is assumed that the size of the transition zone between the H II and H I regions $\Delta R \ll R_{\rm HII}$. Note that a real picture may be more complicated as follows from the theoretical consideration of Grachev (1996).

The innermost parts of the shell are free of dust. If the inner radius of the dusty shell $R_{\rm in}$ is determined by the process of grain sublimation, it should be about 2 – 10 AU depending on the stellar luminosity, the grain composition and size (e.g., Il'in & Voshchinnikov 1993; Friedemann et al. 1994, 1995). We assume that $R_{\rm in} > R_{\rm HII}$. The outer radius of the shell appears to be of some thousand AU (Friedemann et al. 1994, 1995; Krivova & Il'in 1996).

Pressure of radiation of an A-type star is able quickly to sweep submicron dust particles out of the vicinities of the stars. Apparently, the presence of the dusty shells can be explained by the clumps' destruction and an efficient coupling of charged grains with the circumstellar magnetic field (Voshchinnikov & Grinin 1992; Il'in & Krivov 1994).

The estimates made by Voshchinnikov & Grinin (1992) show that the size of the clumps may be ~ 0.2 AU and the orbits of the clumps should have a large eccentricity with the minimum distance from the star of about 5 – 10 AU.

3.2. Density distribution

For a given velocity law $v(R)$, the gas density distribution in the shell can be written as

$$n_{\rm H}(R) = \frac{\dot{M}}{4\pi\mu m_{\rm H} R^2 v(R)}, \qquad (1)$$

where $\dot{M}$ is the mass-loss rate, $\mu \approx 1.35$ the average molecular weight, and $m_{\rm H}$ the mass of an H atom.

We use the standard mass-loss rate $\dot{M} \approx 10^{-8} M_\odot$/yr typical of HAeBe stars. For AB Aur, close values were obtained by CK and Böhm & Catala (1995) from spectral data and by Skinner et al. (1993) from the radio continuum observations of free-free emission.

The velocity law in the shells of HAeBe stars is not well known. Therefore, the standard Lamers law describing the velocity field in the shells of stars of practically all types is adopted

$$v(R) = v_0 + (v_\infty - v_0)\left(1 - \frac{R_\star}{R}\right)^\beta, \qquad (2)$$

where v_0, v_∞, and β are parameters, and $R_\star$ is the stellar radius. The following values of parameters have been used: v_0 = 5 km s^{-1}, v_∞ = 300 km s^{-1} and β = 4. They allow to approximate the average velocity law obtained by CK for the inner layers of the shell surrounding AB Aur (except for a thin layer above the stellar photosphere). Equation (2) gives nearly a constant velocity at $R \geq 1$ AU. Note that there is also an evidence for a deceleration of the wind at larger distances from the stars (Finkenzeller & Mundt 1984).

The density distribution in the clump is presented as

$$n(r) = n(0)\ \exp\left[-\left(\frac{2r}{L^{\rm clump}}\right)^{\eta}\right], \qquad (3)$$

where r is the distance from the clump center, $L^{\rm clump}$ the clump length along the line of sight, $n(0)$ the gas number density at the clump center. Quite different density profiles can be modeled by varying η.

The value of parameter $n(0)$ can be calculated from the extinction produced by a clump and the gas to dust ratio if the size of the clump is much larger than the stellar radius

$$n(0) = \left(\frac{n}{n_{\rm H}}\right)^{-1} \frac{\Delta V^{\rm clump}}{R_V L^{\rm clump}} \left(\frac{N({\rm H})}{E_{B-V}}\right)^{\rm clump} \frac{1}{\Gamma\left(1+\frac{1}{\eta}\right)}, \qquad (4)$$

where $n_{\rm H}/n$ = 0.936 is the relative abundance of hydrogen, $\Delta V^{\rm clump}$ the visual extinction in the clump[1], $N({\rm H})/E_{B-V}$ the gas to dust ratio, $R_V = \Delta V^{\rm clump}/E_{B-V}$, and $\Gamma(z)$ is the Gamma function.

The possible presence of a very dense core or an asteroid-size body at the center of the clump (Friedemann et al. 1995; Kholtygin 1995) should not change its ionization structure.

3.3. Temperature distribution

The semi-empirical model of CK used by us includes a chromosphere, the thin hot layer near the star. The temperature distribution has a maximum ($\approx$ 17000 K) at $R \approx 1.08 R_\star$ and a rapid decrease down to about 3000 – 8000 K outside the chromosphere boundary ($R_{\rm ch} \approx 1.5\, R_\star$).

The H II region is supposed to be isothermal. The narrow ($\sim$ 0.01 AU) layer above the chromosphere where the temperature rapidly drops down is treated following CK.

The gas temperature in the C II region decreases outward from $\sim$ 8000 K to $\sim$ 1000 K (see, e.g., Berrilli et al. 1992). In our model, the C II region is isothermal but its temperature, $T_{\rm CII}$, is a model parameter.

It is evident that the C I region must be colder than the C II region. As the ionization structure of both regions is practically independent of the gas temperature, one can accept that $T_{\rm CI} = T_{\rm CII}$.

A consideration of the gas thermal equilibrium in the clumps (see Appendix A) shows that the gas temperature $T^{\rm clump}$ should lay between about 200 K and 1000 K. At present, a more detailed analysis does not seem to be reasonable since the description of some processes (e.g. photoelectron emission) is rather approximate and the physical conditions in the clumps are unclear. Therefore, we assume the clumps to be isothermal with $T^{\rm clump}$ being in the range given above.

[1] It is equal to the decrease of stellar brightness if the projected clump size is larger than the stellar diameter (see Sect. 4.3.1).

Table 1. Cosmic abundances and depletions of the elements with the ionization potential $I_{\rm p} < 13.6$ eV

Element	Abundance	$I_{\rm p}$ (eV)	$\mathscr{D}_{\rm X}$ warm interstellar medium	$\mathscr{D}_{\rm X}$ cold interstellar medium
C	$4.4\,10^{-4}$	11.260	−0.3	−0.8
Na	$2.3\,10^{-6}$	5.139	−0.5	−0.7
Mg	$4.0\,10^{-5}$	7.646	−0.2	−0.7
Al	$3.2\,10^{-6}$	5.986	−1.0	−2.0
Si	$3.8\,10^{-5}$	8.151	−0.6	−1.6
S	$1.9\,10^{-5}$	10.360	~ 0	−0.7
Ca	$2.4\,10^{-6}$	6.113	−1.2	−3.6
Fe	$3.4\,10^{-5}$	7.870	−1.2	−2.0
Ni	$1.8\,10^{-6}$	7.635	−1.4	−2.0

3.4. Ionization equilibrium

3.4.1. Atoms and lines

As the ionization equilibrium in an H I region is studied, the elements with an ionization potential $I_{\rm p} \leq 13.6$ eV are taken into account. The list of low-potential elements with cosmic abundances relative to hydrogen larger than 10^{-6} according to Cameron (1982) is given in Table 1. In H I regions, only the calcium can be twice ionized ($I_{\rm p}$(Ca II) = 11.871 eV).

Some of the elements considered may be strongly depleted being incorporated into dust grains. The depletion of element X is

$$\mathscr{D}_{\rm X} = \log\left(\frac{N_{\rm X}}{N_{\rm H}}\right) - \log\left(\frac{N_{\rm X}}{N_{\rm H}}\right)_\odot, \qquad (5)$$

where $N_{\rm X}/N_{\rm H}$ and $(N_{\rm X}/N_{\rm H})_\odot$ are the observed and Solar system abundances relative to hydrogen. The values of $\mathscr{D}_{\rm X}$ published by Turner (1991) for the cold interstellar medium and by de Boer et al. (1987) for the warm diffuse medium are given in Table 1.

The characteristics of the strongest optical and ultraviolet resonance lines of the ions under consideration are collected in Table 2, where the last column gives the oscillator transition strengths.

3.4.2. Equation of ionization equilibrium

The following processes mainly affect the ionization balance of the gas in the shell: photoionization, ionization by cosmic-ray particles, photorecombination and dielectronic recombination.

Table 2. Resonance lines of the most abundant ions with the ionization potential $I_p < 13.6$ eV

Ion	λ (Å) [(a)]	Transition	Multiplet	$f_{JJ'}$ [(b)]
Na I D_2	5889.95	$3s - 3p$	$^2S_{1/2} - {}^2P^0_{3/2}$	1.31
D_1	5895.92	$3s - 3p$	$^2S_{1/2} - {}^2P^0_{1/2}$	0.65
Mg I	2852.13	$3s^2 - 3s3p$	$^1S_0 - {}^1P^0_1$	1.6
Al I	3944.01	$3p - 4s$	$^2P^0_{1/2} - {}^2S_{3/2}$	0.23
	3961.52	$3p - 4s$	$^2P^0_{3/2} - {}^2S_{3/2}$	0.46
Si I	2506.90	$3p^2 - 3p4s$	$^3P_1 - {}^3P^0_2$	0.06
	2514.32	$3p^2 - 3p4s$	$^3P_0 - {}^3P^0_1$	0.16
	2516.11	$3p^2 - 3p4s$	$^3P_2 - {}^3P^0_2$	0.12
	2519.20	$3p^2 - 3p4s$	$^3P_1 - {}^3P^0_1$	0.04
	2524.11	$3p^2 - 3p4s$	$^3P_1 - {}^3P^0_0$	0.05
	2528.51	$3p^2 - 3p4s$	$^3P_2 - {}^3P^0_1$	0.04
Ca I	4226.73	$4s^2 - 4s4p$	$^1S_0 - {}^1P^0_1$	1.75
Ca II K	3933.7	$4s - 4p$	$^2S_{1/2} - {}^2P^0_{3/2}$	1.38
H	3968.5	$4s - 4p$	$^2S_{1/2} - {}^2P^0_{1/2}$	0.69
Fe I	3820.4	$3d^74s - 3d^74p$	$^5F_5 - {}^5D^0_4$	0.16

[(a)] Striganov & Odintsova (1982)
[(b)] Morton (1991)

The ionization by electron collisions is very weak because of the low electron temperature. The charge transfer reactions are also unimportant as their rates are rather slow at the temperatures considered (Golovatyj et al. 1991). The emission of photoelectrons from the grain surfaces becomes significant if the ionization degree $< 10^{-6}$ (Nishi et al. 1991). It is also evident that molecules in the clumps cannot be a source of additional electrons because their ionization potentials are too high. Therefore, we have neglected all these processes.

Thus, the equations of ionization equilibrium in the H I region of the shells can be written as follows

$$\begin{cases} \zeta_H n_H &= \alpha^{rr}_{H^+} n_e n_{H^+} \\ \Gamma_X n_X &= (\alpha^{rr}_{X^+} + \alpha^{dr}_{X^+}) n_e n_{X^+}, \end{cases} \quad (6)$$

where ζ_H is the rate of ionization by cosmic rays, Γ_X the photoionization rate for element X, $\alpha^{rr}_{X^+}$ and $\alpha^{dr}_{X^+}$ are the radiative and dielectronic recombination rates, n_X and n_{X^+} the density of neutral and ionized atoms, respectively, and n_e is the electron density. The approximations of the rates used in our calculations are described in Appendices B and C. In the calculations we used the standard value of the ionization rate $\zeta_H = 10^{-16}\,s^{-1}$ (Spitzer & Jenkins 1975).

Equations (6) were supplemented by the conditions of charge and gas density conservation and solved iteratively from the H II region boundary outward. The obtained column density and ion number density were used to calculate the equivalent width of the spectral lines in the frame of the "quasi-nebular" approximation (see Appendix D for details).

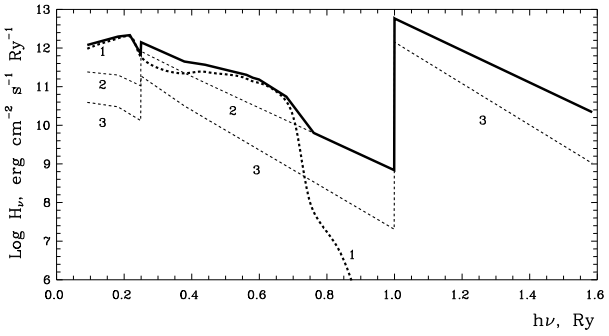

Fig. 1. Spectrum of ionizing radiation in the shell of a Herbig Ae/Be star. Dashed lines show the contributions to the total flux from the stellar photosphere (1), the chromosphere (2) and the H II region (3)

3.4.3. Ionizing radiation

The radiation ionizing atoms is the sum of the radiation of the stellar photosphere, the chromosphere, and the H II region surrounding the star.

For the stellar photosphere, the standard LTE models were used (Kurucz 1979). Note that these models show a steep decrease of the flux at $\lambda \approx 1200$ Å and, therefore, at shorter wavelengths the spectrum of ionizing radiation should be determined by the chromosphere and/or the H II region. The fluxes for the Kurucz model with $T_\star = 9000$ K and $\log g = 4.0$ are plotted in Fig. 1. We adopt that the star has the luminosity $L_\star = 40 L_\odot$. Then, its radius and mass are: $R_\star \approx 2.6 R_\odot \approx 1.8\,10^{11}$ cm and $M_\star = 2.5 M_\odot$, respectively. Considering the stellar chromosphere, we base on the semi-empirical model developed by CK. Since the gas temperature is relatively low (≤ 17000 K), the ionizing radiation is a result of free-free and free-bound emission of hydrogen. Other ionized atoms can be neglected because of their small abundances. The total luminosity of the chromosphere at the frequency ν is

$$L^{ch}_\nu = 4\pi \int_{R_\star}^{R_{ch}} R^2\, n^2_H(R)\, \varepsilon_\nu(R)\, dR\,, \quad (7)$$

where $\varepsilon_\nu(R) = \varepsilon_\nu\Big(T_e(R)\Big)$ is the hydrogen emission coefficient, and all hydrogen atoms in the chromosphere are assumed to be ionized ($n_e = n_H$). The method used for the calculations of the emission coefficient is described in Appendix E.

The equation similar to Eq. (7) is applied to calculate the luminosity of the H II region, but in this case, the density distribution given by Eqs. (1), (2) and a constant temperature are taken. The fluxes from the chromosphere and the H II region referred to the level of the photosphere $H_\nu = L_\nu / 4\,\pi\, R^2_\star$ are plotted in Fig. 1. For given density and velocity distributions (see Eqs. (1) and (2)), the flux H^{HII}_ν weakly depends on R_{HII}. Therefore, in our calculations we used $R_{HII} = 1$ AU.

The flux of ionizing radiation outside the H II region (both in the shell and in the clumps) can be approximated as

$$H_\nu \approx \mathscr{W}\,(H^{ph}_\nu + H^{ch}_\nu + H^{HII}_\nu)\, \exp\left[-(\tau^{dust}_\nu + \tau^{gas}_\nu)\right]. \quad (8)$$

Here, $\mathscr{W}$ is the radiation dilution factor, $\tau_\nu^{\rm dust}$ and $\tau_\nu^{\rm gas}$ are the optical thickness caused by the dust extinction and the gas continuous absorption, respectively. The latter is

$$\tau_\nu^{\rm gas} = \sum_{\rm X} \int_{R_{\rm HII}}^{R} n_{\rm X} \sigma_\nu^{\rm X}\, dR, \qquad (9)$$

where $\sigma_\nu^{\rm X}$ is the photoionization cross-section of element X (see Eq. (B2)). Other sources of opacity (H^-, H+H, etc.) are unimportant at wavelengths shorter than 2400 Å that corresponds to the ionization threshold of Na, the atom with the lowest ionization potential (see Table 1).

We consider the optically thin shells ($\tau^{\rm dust} < 0.5$), but the fraction of radiation scattered by dust may still be substantial. The calculations of Voshchinnikov et al. (1995) show that the ratio of the scattered radiation to the stellar one is about 0.2 – 0.3 at wavelengths $\sim$ 1000 – 2000 Å. The negligence of the scattered radiation in Eq. (8) leads to overestimating the neutral atom density, but this effect is weak. The diffuse L_α-radiation can be also neglected since L_α-photons would be absorbed by dust particles both in the C II and C I regions.

3.5. Dust grains

The expression of the optical thickness of a dusty layer can be written using the gas to dust ratio $N({\rm H})/E_{B-V}$ and the gas column density $N({\rm H})$

$$\tau_\lambda^{\rm dust} = \frac{R_V}{1.086}\,\frac{A_\lambda}{A_V}\,\left(\frac{N({\rm H})}{E_{B-V}}\right)^{-1} N({\rm H}), \qquad (10)$$

where A_λ/A_V is the normalized extinction curve and R_V the ratio of the total to selective extinction.

The interpretation of photometric and polarimetric observations of HAeBe stars indicates that the properties of circumstellar grains may differ from those of interstellar grains (Voshchinnikov et al. 1988, 1995, 1996). In our modelling, we used the dust mixture found for the shell around WW Vul by Voshchinnikov & Grinin (1992): the minimum grain size $a_- = 0.055\ \mu$m, the maximum grain size $a_+ = 0.25\ \mu$m, the slope of the size distribution $q = 5$ ($n_{\rm dust} \propto a^{-q}$), the ratio of graphite to silicate grains $n_{\rm C}/n_{\rm Si} = 4$. For this mixture, the ratio of the total to selective extinction is $R_V \approx 3.8$. Note that the parameters of the dust mixture diverse from those of the standard MRN one ($a_- \approx 0.005\ \mu$m, $q \approx 3.5$, $n_{\rm C}/n_{\rm Si} \approx 1$). Following Voshchinnikov & Grinin (1992), it is also assumed that the properties of the dust grains in the shell and clumps are the same.

3.6. Model parameters

The main parameters of our model presented in Table 3 are divided among two groups: the shell and clump parameters. They were varied within plausible boundaries. The standard values of the parameters are given in the last column of Table 3.

The element depletions in the clumps are assumed to be similar to those for the warm interstellar medium (see Table 1) as the clumps look to be fast moving warm objects. In the interclump medium of the shells the element abundances are taken to be normal ($\mathscr{D}_{\rm X} = 0$).

Table 3. Model parameters and their standard values

Parameter	Designation	Standard value
Shell		
Mass loss rate	$\dot{M}$	$10^{-8}\ M_\odot$
Gas temperature:		
H II region	$T_{\rm HII}$	8000 K
C II region	$T_{\rm CII}$	3000 K
C I region	$T_{\rm CI}$	3000 K
Gas to dust ratio	$\frac{N({\rm H})}{E_{B-V}}$	$5\,10^{21}$ cm^{-2}mag^{-1}
Element depletion	$\mathscr{D}_{\rm X}$	0
Gas turbulent velocity	$v_{\rm turb}$	5 km s^{-1}
Inner radius	$R_{\rm in}$	7 AU
Clump		
Visual extinction	$\Delta V^{\rm clump}$	$2\overset{\rm m}{.}0$
Length	$L^{\rm clump}$	0.2 AU
Density profile	η	3
Distance from star	$R^{\rm clump}$	10 AU
Gas temperature	$T^{\rm clump}$	500 K
Gas to dust ratio	$\left(\frac{N({\rm H})}{E_{B-V}}\right)^{\rm clump}$	$5\,10^{21}$ cm^{-2}mag^{-1}
Element depletion	$\mathscr{D}_{\rm X}^{\rm clump}$	warm interstellar medium
Gas turbulent velocity	$v_{\rm turb}^{\rm clump}$	1 km s^{-1}

4. Results and discussion

The local electron and ion density of the elements given in Table 1 have been calculated for a wide range of the parameter values. In this paper, the data for sodium and calcium producing the strongest visual lines (see Table 2) are examined, other results will be presented elsewhere.

4.1. Local density and ionization degree

The obtained electron density and the relative abundances of ions $n({\rm C\,I})/n({\rm C})$, $n({\rm Na\,I})/n({\rm Na})$, and $n({\rm Ca\,II})/n({\rm Ca})$ are presented in Fig. 2. They were calculated for two models with a different degree of the matter concentration in the clumps (see the upper part of the figure). Variations of the relative abundances outside the zone shown in Fig. 2 are rather small. In the shadows produced by the clumps the fractions of C I, Na I and Ca II are slightly higher than ahead of them.

From Fig. 2 one can see that carbon, sodium and calcium in the interclump medium are mainly in the state of the C II, Na II, and Ca III ions. Note that the calcium is twice ionized and the size of the C II region is rather large because the ionizing radiation of the chromosphere was included in our model.

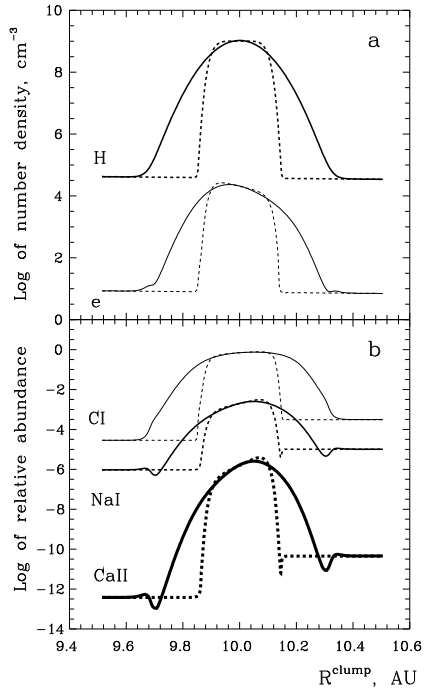

Fig. 2a and b. The hydrogen and electron number density (**a**) and the relative abundances of ions: n(C I)/n(C), n(Na I)/n(Na), and n(Ca II)/n(Ca) in the shell with the clump (**b**). The centers of the clumps with the moderate (η = 2; see Eq. (3); solid lines) and strong (η = 6; dashed lines) matter concentration are located at the distance of 10 AU from the star. The values of other parameters are as in Table 3

The ionization degree of the gas in the shell outside the clumps is $n_e/n \approx (2-4)\,10^{-4}$ and practically does not depend on the distance from the star up to $R \approx 60$ AU. At larger distances, the ionization of hydrogen by cosmic rays starts to increase the ionization degree.

In the clumps, the ionization degree is mainly determined by the gas density and the distance of the clump from the star (see Fig. 3). The values of $n(0)$ shown in Fig. 3a were obtained by variations of the gas to dust ratio in Eq. (4). For the model with the values of parameters from Table 3, $n(0) \approx 1.05\,10^9$ cm^{-3}. A similar (but not the same) dependence occurs if we increase $\Delta V^{\rm clump}$ or decrease $L^{\rm clump}$. The knees seen in Fig. 3b are related to the narrow layer where the diffuse dust appears in the shell ($R \approx R_{\rm in}$).

4.2. Lines forming in the shell

If there are no clumps in the line of sight, the absorption lines should be blueshifted with the typical wind velocity. Our calculations made with the standard values of the parameters demonstrate that the column density of Na I and Ca II are small and the lines should be extremely weak (see the last row of Table 4).

In our model, the shell lines are mainly formed at the distances $\sim 1-5$ AU where only the negligible part of sodium and calcium is in the state of Na I and Ca II. In order to enlarge the amount of neutral sodium and the Ca II ion one can decrease the ionizing flux or/and increase the gas density. The latter may be made if we invoke an anisotropy or a strong deceleration of the wind, or possibly a shock where the stellar wind encounters the surrounding envelope.

As our calculations show, if the final wind velocity is as low as $v_\infty = 5$ km s^{-1} the absorption lines can become rather strong (see Table 4). However, in this case it is difficult to explain the lines highly shifted from their rest wavelengths and the short-time line variability.

4.3. Lines forming in clumps

Some results of our calculations for the models with a clump in the line of sight are presented in Table 5. The values of the parameters which are not mentioned there have been chosen to be equal to the standard values given in Table 3. The changes of the density distribution in the clump (the parameter η) influence the results only slightly and are not illustrated in Table 5.

Some model parameters listed in Table 3 affect the results strongly. This group includes the gas to dust ratio, the element depletion and the velocity of large-scale gas motions. At present, the values of these parameters are unknown, and they could be estimated from a comparison of the calculated and observed equivalent width of the Na I and Ca II lines. The results presented in Table 5 demonstrate that the saturated lines of Na I and Ca II can be formed in the clumps, and that the lines could be observed with the current telescopes.

It should be noted that the calculated column density of Na I and Ca II are of the same order. This result would change drastically provided we neglect the radiation of the chromosphere and the H II region. In this case, calcium will be mainly in the state of the Ca II ion, and the lines of the ion will be considerably enhanced in comparison with the sodium lines. Such a model including only the photospheric radiation has been considered by Sorelli et al. (1996).

4.3.1. Large and small clumps

If the projected size of the clump is comparable with the stellar diameter ($D^{\rm clump} \gtrsim 2R_\star$), the correlation between the stellar brightness variations and the behaviour of the absorption lines should be expected. Then, the data from Table 5 may be used to estimate some characteristics of large clumps.

However, in many cases large variations of the absorption components of the sodium and calcium lines are not accompanied by significant brightness variations (see, e.g., Fig. 5 in the paper of Grinin et al. 1994). In order to damp down the brightness variations, the projected size of the clump must be much smaller than the stellar diameter. If the observed variation of stellar brightness is $\Delta V^{\rm obs}$, then the upper limit to the clump size is

$$D^{\rm clump} \lesssim 2\,R_\star \left(\frac{\Delta V^{\rm obs}}{\Delta V^{\rm clump}}\right)^{1/2} \approx$$
$$\approx 0.0054 \left(\frac{0.1\,\text{mag.}}{\Delta V^{\rm obs}}\right)^{1/2} \left(\frac{\Delta V^{\rm clump}}{2.0\,\text{mag.}}\right)^{1/2} \text{AU}. \qquad (11)$$

Table 4. Dependence of column density, line optical thickness and equivalent width on the terminal wind velocity

v_∞, km s^{-1}	log N(Na I) (cm^{-2})	log τ_0(Na I D_2)	W(Na I D_2) (Å)	log N(Ca II) (cm^{-2})	log τ_0(Ca II K)	W(Ca II K) (Å)
5	11.87	0.23	0.1804	12.37	0.58	0.1722
10	11.28	– 0.37	0.0662	11.78	– 0.01	0.0834
30	10.33	– 1.31	0.0084	10.83	– 0.96	0.0124
100	9.29	– 2.36	0.0008	9.79	– 2.01	0.0012
300	8.33	– 3.31	0.0001	8.84	– 2.96	0.0001

Table 5. Dependence of column density, line optical thickness and equivalent width on model parameters

Parameter	log N(Na I) (cm^{-2})	log τ_0(Na I D_2)	W(Na I D_2) (Å)	log N(Ca II) (cm^{-2})	log τ_0(Ca II K)	W(Ca II K) (Å)
$\Delta V^{\rm clump}$						
$0\overset{\rm m}{.}2$	10.44	– 0.54	0.010	10.27	– 0.85	0.003
$0\overset{\rm m}{.}5$	11.23	0.25	0.040	11.05	– 0.06	0.016
$1\overset{\rm m}{.}0$	11.85	0.88	0.067	11.68	0.56	0.035
$2\overset{\rm m}{.}0$	12.54	1.56	0.086	12.36	1.25	0.050
$3\overset{\rm m}{.}0$	13.01	2.03	0.097	12.83	1.71	0.058
$L^{\rm clump}$, AU						
0.001	14.00	3.03	0.117	13.95	2.84	0.074
0.01	13.29	2.32	0.103	13.10	1.99	0.062
0.1	12.72	1.74	0.091	12.54	1.43	0.054
0.2	12.54	1.56	0.086	12.36	1.25	0.050
1.0	12.09	1.12	0.074	11.91	0.80	0.041
$T^{\rm clump}$, K						
200	12.39	1.44	0.079	12.22	1.12	0.047
500	12.54	1.56	0.086	12.36	1.25	0.050
1000	12.88	1.87	0.101	12.69	1.56	0.058
$\left(N({\rm H})/E_{B-V}\right)^{\rm clump}$, cm^{-2}mag^{-1}						
$5\,10^{21}$	12.54	1.56	0.086	12.36	1.25	0.050
$5\,10^{22}$	14.11	3.14	0.119	13.93	2.82	0.073
$5\,10^{23}$	15.68	4.71	0.144	15.48	4.37	0.090
$\mathscr{D}_{\rm Na}^{\rm clump}$						
– 0.7	12.33	1.36	0.081	—	—	—
– 0.5	12.54	1.56	0.086	—	—	—
0.0	13.11	2.14	0.100	—	—	—
$\mathscr{D}_{\rm Ca}^{\rm clump}$						
– 3.6	—	—	—	10.00	–1.15	0.002
– 1.2	—	—	—	12.36	1.25	0.050
0.0	—	—	—	13.63	2.52	0.069
$v_{\rm turb}^{\rm clump}$, km s^{-1}						
1	12.54	1.56	0.086	12.36	1.25	0.050
5	12.54	0.90	0.312	12.36	0.57	0.169
10	12.54	0.60	0.519	12.36	0.27	0.249
50	12.54	– 0.98	1.070	12.36	– 0.43	0.382

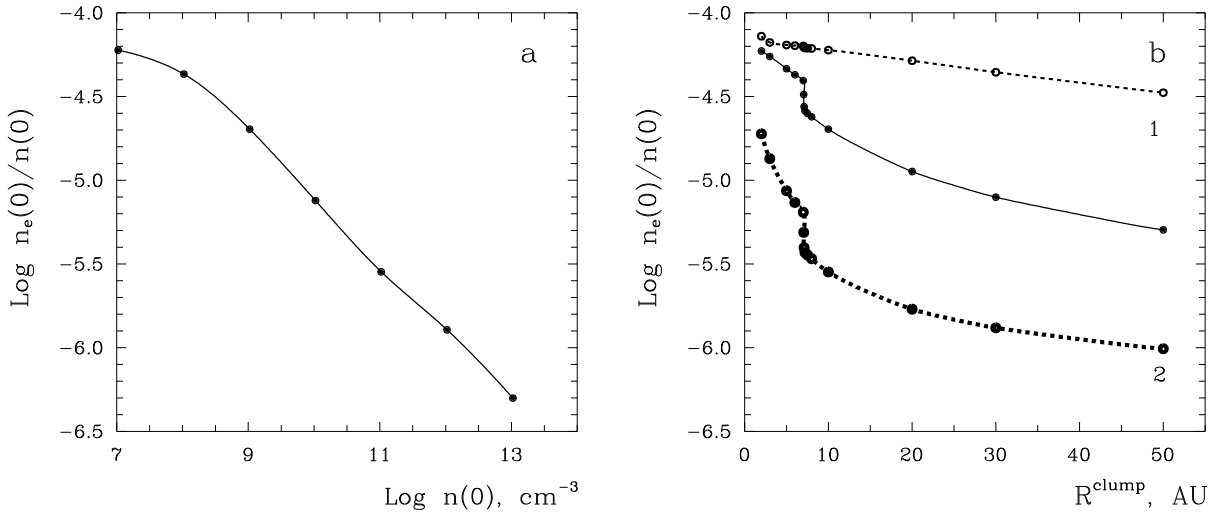

Fig. 3a and b. The ionization degree at the clump center. **a** The clump is located at the distance $R^{\rm clump}$ = 10 AU. The values of $n(0)$ correspond to the gas to dust ratios $\left(\frac{N({\rm H})}{E_{B-V}}\right)^{\rm clump}$ = 5 10^{21} – 5 10^{25} cm^{-2}mag^{-1}. **b** Solid line: $n(0)$ = 1.05 10^{9} cm^{-3}; dashed lines: 1 – $n(0)$ = 1.05 10^{7} cm^{-3}; 2 – $n(0)$ = 1.05 10^{11} cm^{-3}. The values of other parameters are as in Table 3

The numerical coefficient in Eq. (11) is obtained if we accept the standard value of $\Delta V^{\rm clump}$ = $2\overset{\rm m}{.}0$ (Table 5) provided the observed star obscuration is $\Delta V^{\rm obs} \lesssim 0\overset{\rm m}{.}1$. If the size of the clump is equal to its length, i.e. $L^{\rm clump} = D^{\rm clump}$ = 0.0054 AU, the gas density at the clump center is $n(0) \approx 3.90\,10^{10}$ cm^{-3}. The lines forming in such a clump would be rather strong (see Table 5). Their variability may be connected with the changes of the physical conditions in the moving clump (turbulent velocity, element depletion).

4.3.2. Clumps at different distances

The equivalent width of the sodium and calcium lines for the clumps located at different distances from the star are presented in Fig. 4. The solid lines show the results of calculations for the model with the standard values of parameters (see Table 3). The different values of W obtained are connected with the decrease of the ionizing radiation flux with distance (see Eq. (8)). The dashed lines were calculated for the model where the turbulent velocity is inversely proportional to the distance: $v_{\rm turb}^{\rm clump} \propto (R^{\rm clump})^{-1}$ with $v_{\rm turb}^{\rm clump}$ = 1 km s^{-1} at $R^{\rm clump}$ = 50 AU and $v_{\rm turb}^{\rm clump}$ = 10 km s^{-1} at $R^{\rm clump}$ = 2 AU. The latter value of $v_{\rm turb}^{\rm clump}$ can be estimated from the width of the calcium and sodium lines ($v_{\rm turb}^{\rm clump} \approx$ FWHM/1.66; Kaplan & Pikel'ner 1979) observed by Catala et al. (1986a). The turbulent velocity increasing with the decrease of $R^{\rm clump}$ leads to the growth of W when $R^{\rm clump} \gtrsim 10$ – 15 AU. Closer to the star, a significant increase of the flux of ionizing radiation occurs. This results in a decline of the number of neutral sodium and Ca II ions. Note that the destruction of dust grains in the clumps may produce additional Na and Ca atoms that could change the element depletion and increase the gas to dust ratio.

4.3.3. Moving clumps

The behaviour of the absorption lines in spectra of HAeBe stars should depend on the clump orbits (radial velocities) and the physical conditions in the clumps (the width and strength of the lines). In the above discussion, the latter topic has been treated. Now, we consider some problems related to the clump orbital motion.

It is naturaly to adopt that the periastron of the clump orbit lies between the star and an observer, and the line of apsides does not coincide with the line of sight. Evidently, a very small part of the clump orbit only is projected on the stellar disk and can be observable.

When a clump moving from the distant circumstellar environments appears on the stellar disk, the absorption line should be blueshifted and narrow. Closer to the periastron, the radial velocity drops down to a minimum value. Because of the growth of the turbulent velocity, the line width should increase. Meantime, the growing number of ions may make the line deeper.

If a clump is observed after its passage of the periastron, the line is expected to be redshifted. The redshifted components must be broader than the blueshifted ones because the clump was disturbed near the star. Note that very wide lines may be a result of the presence of several clumps in the line of sight. The numerous mechanisms of clump destruction operating near HAeBe stars (see Friedemann et al. 1995 and Mitskevitch 1995 for discussion) can cause the fragmentation and destruction of large clumps in the immediate stellar environments. It is expected that after the periastron the fragments continue their way moving away from the star or falling onto them. In both cases, the absorption lines should be redshifted.

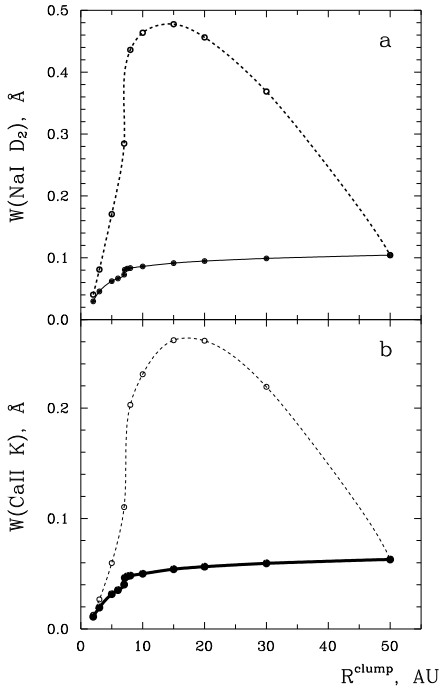

Fig. 4a and b. The equivalent width of the sodium (**a**) and calcium (**b**) lines in dependence on the clump distance to the star. Solid lines: $v_{\rm turb}^{\rm clump}$ = 1 km s^{-1}. Dashed lines: $v_{\rm turb}^{\rm clump} \propto (R^{\rm clump})^{-1}$, where $v_{\rm turb}^{\rm clump}$ = 1 km s^{-1} at $R^{\rm clump}$ = 50 AU and $v_{\rm turb}^{\rm clump}$ = 10 km s^{-1} at $R^{\rm clump}$ = 2 AU. The values of other parameters are as in Table 3

4.3.4. 90 km s^{-1} component in the spectrum of AB Aur

Some speculative estimates of the clump orbit can be made from the observations of AB Aur made in December 1991 by Catala et al. (1993). The authors observed the absorption components of the Na I D, Ca II K and Fe II lines blueshifted by $\sim$ 90 km s^{-1}. The equivalent width of the sodium and iron lines was $W \approx 0.03 - 0.10$ Å (Catala 1996). It was found that the lifetime of the 90 km s^{-1} component was longer than 24 hours (from the observations of the Na I D lines, $t_{\rm NaI} \gtrsim 24^{\rm h}$), but less than 67 hours (from the observations of the Fe II lines, $t_{\rm FeII} \lesssim 67^{\rm h}$). We attribute the first interval to the time of the sodium ionization. Then, the upper limit to the electron density inside the clump is

$$n_e \lesssim \frac{1}{\alpha_{\rm NaI}^{\rm rr} t_{\rm NaI}} \approx 6.9\,10^6\,{\rm cm}^{-3}. \quad (12)$$

Here, $\alpha_{\rm NaI}^{\rm rr}$ is the rate of radiative recombination of neutral sodium given by Eq. (B1). The numerical value was calculated for $T^{\rm clump}$ = 500 K.

The photometric history of AB Aur gives evidence that its visual brightness was varying considerably in thirties (see discussion in Voshchinnikov et al. 1996). A far infrared variability has been found by Prusti & Mitskevitch (1994). Clumps may be responsible for both effects. However, during many last years the brightness of the star is stable. Then, the size of the clump producing the – 90 km s^{-1} component must be small (see Eq. (11)). As follows from Fig. 3, a clump with the central density in the limits $n(0) \approx 10^7 - 10^{11}$ cm^{-3} satisfies the condition of Eq. (12). The clump's location in the shell may be arbitrary between 2 AU and 50 AU in our model. However, the value of $R^{\rm clump}$ near the lower limit (2 AU) seems to be more probable because the observed equivalent width W(Na I D$_2$) = 0.03 – 0.05 Å may be easily reproduced in this case (see Fig. 4).

The second time, $t_{\rm FeII}$, may be connected with the time of clump's crossing the stellar disk. The tangential component of the clump velocity is

$$v_t^{\rm clump} \approx \frac{2R_\star}{t_{\rm FeII}} \approx 15\,{\rm km\,s}^{-1}. \quad (13)$$

The total clump velocity

$$v^{\rm clump} = \sqrt{(v_t^{\rm clump})^2 + (v_r^{\rm clump})^2} \approx 91\,{\rm km\,s}^{-1} \quad (14)$$

allows to estimate the type of Keplerian orbit. A body moving near a star is known to have an elliptic orbit (see, e.g., Roy 1978) if

$$v^{\rm clump} < \left(\frac{2GM_\star}{R^{\rm clump}}\right)^{1/2} \approx 47\,{\rm km\,s}^{-1}. \quad (15)$$

Here, we used the value of $R^{\rm clump}$ = 2 AU. So, we can conclude that the clump orbit seems to be hyperbolic.

4.3.5. Ten days absorption event in the spectrum of HR 5999

For HAeBe star HR 5999 Tjin A Djie et al. (1989) published the radial velocities and the equivalent width of sodium, calcium, iron and other lines together with the simultaneous photometry. Here, we interpret the behaviour of W(Na I D$_2$) within a ten days period: from 21.05.78 till 01.06.78. In this time, there were made 9 observations and the stellar brightness decreased from $V = 6\overset{\rm m}{.}9$ to $7\overset{\rm m}{.}2$. The variations of the radial velocity and the equivalent width with brightness are shown in Fig. 5 by open circles. The observations obtained on the sequent dates are connected by dashed line.

For our modelling, we choose the photospheric fluxes corresponding to the Kurucz (1979) model with the parameters $T_\star$ = 7800 K and $\log g$ = 3.5 which are close to those adopted for HR 5999 (Thé et al. 1994). The changes of v_r could be explained as an absorption in the clump approaching the periastron. However, the distance that the clump can pass during ten days is too small to expect large changes of the ionizing flux and the sodium abundance. Therefore, we treat the observed variations of W(Na I D$_2$) as a result of the stellar obscuration by a clump with a variable turbulent velocity which is smaller in its denser parts and larger in its rarefied parts. The density profile may look like that shown in Fig. 2 for the clump with a moderate gas concentration. The observed slope of data can be reproduced if we take the value $v_{\rm turb}^{\rm clump}$ = 6 km s^{-1} in the outer parts of the clump and $v_{\rm turb}^{\rm clump}$ = 2 km s^{-1} in the inner ones. The observations could be fitted better if one chooses the gas to dust ratio $\left(\frac{N({\rm H})}{E_{B-V}}\right)^{\rm clump} = 5\,10^{23}$ cm^{-2}mag^{-1}, that is two orders larger than the standard interstellar one.

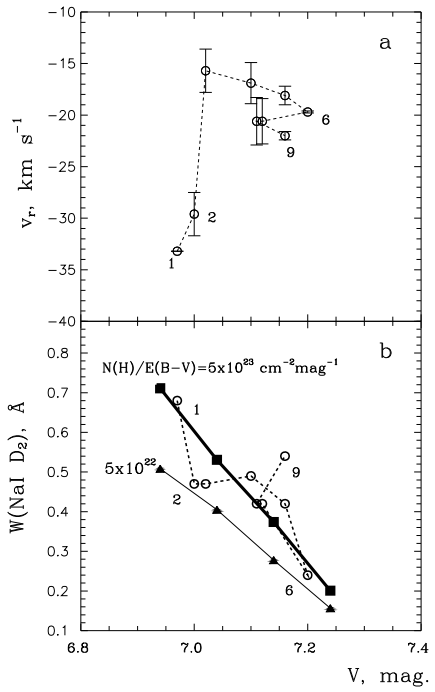

Fig. 5a and b. The behaviour of the radial velocity (**a**) and the equivalent width (**b**) of the Na I D_2 line in the spectrum of HR 5999. Numbers denote the observations made in the sequent dates. Filled signs show the results of model calculations for two values of the gas to dust ratio in the clump with $v_{\rm turb}^{\rm clump}$ = 6 km s^{-1} in its outer part and $v_{\rm turb}^{\rm clump}$ = 2 km s^{-1} in the inner part

5. Conclusions

The ionization equilibrium of the gas in the shells surrounding Herbig Ae/Be stars has been studied. The opaque circumstellar dust clumps which could be responsible for the brightness variations of these stars were included in the consideration.

The column density of the ions C I, C II, Ca I, Ca II, Ca III, Na I, Na II and the equivalent width of the Na I D_2 and Ca II K lines have been calculated. It was found that in the shells without clumps strong lines could originate if the gas density is enhanced, for example, because of a strong deceleration of the wind. But the lines is expected to be slightly shifted from their rest wavelengths.

The lines forming in the clumps at the distances larger than several AU from the star must have variable profiles. They can be either blueshifted or redshifted in dependence on the clump orbit orientation relative to the line of sight. It was shown that the column density and equivalent width were mainly determined by clump opacity, the gas to dust ratio, the element depletion and the velocity of large-scale turbulent motions in the clump. If the size of the clump is large enough, appearance (or strengthening) of absorption lines should be accompanied by stellar brightness variations.

Acknowledgements. We are thankful to V.P. Grinin who initiated this work, A.G. Kritsuk for consideration of the thermal balance of gas, S.I. Grachev for helpful discussions, and J. Gürtler for suggestions improved the text. Special thanks to Claude Catala, the referee, for many valuable comments and for sending the unpublished results. V.B.I. acknowledges the support from the Alexander von Humboldt Foundation. The work was partly supported by the ESO C&EE Programme (grant A-01-093).

Appendix A: thermal equilibrium

The gas temperature inside the clump can be determined from the solution to the thermal balance equation

$$\mathscr{G} = \mathscr{L}, \tag{A1}$$

where $\mathscr{G}$ and $\mathscr{L}$ are the heating and cooling rates. The main gain in the heating is provided by electrons from the photoionization of the neutral carbon ($\mathscr{G}_1$) and the photoelectron emission from the surfaces of dust grains ($\mathscr{G}_2$). The contribution of the atomic carbon photoionization to the heating is (e.g., Rudzikas et al. 1991)

$$\mathscr{G}_1 = \int_{\nu_{\rm ph}}^{\infty} \sigma_\nu^{\rm C} \, \frac{4\pi J_\nu}{h\nu} \, (h\nu - h\nu_{\rm ph}) \, d\nu. \tag{A2}$$

Here, $\nu_{\rm ph} = I_{\rm p}/h$ is the threshold frequency, J_ν the mean intensity. The approximation of the photoionization cross-section $\sigma_\nu^{\rm C}$ is given by Eq. (B2).

The photoelectron emission from dust grains has been treated according to Tielens & Hollenbach (1985).

Using the expressions from Draine (1978) and Tielens & Hollenbach (1985), the heating caused by the photodissociation and photoexcitation of the H_2 molecules by the UV radiation has been also estimated. The rôle of this effect is rather small for the clumps with the considered values of parameters.

At the temperatures $T \lesssim 1000$ K, the main source of the gas cooling appears to be the line emission of atoms and ions which are excited by electron impacts. Then, the gas cooling rate is equal to

$$\mathscr{L} = \sum_{k>i} n_k \, A_{ki} \, \Delta E_{ik} \, . \tag{A3}$$

Here, n_k is the occupancy of the level k, A_{ki} the $k \to i$ transition probability and ΔE_{ik} the energy of the transition. Note that all transitions between the fine structure levels of the ion are summed. The following atoms and ions have been included in the calculations: H, C, C$^+$, N, O, S, S$^+$, Fe and Fe$^+$. The values of n_k have been found as the solutions to the statistical balance equations. The rates of the radiative and collisional transitions were obtained from the atomic constants published by Tielens & Hollenbach (1985) and Golovatyj et al. (1991).

Other sources of the gas cooling are not expected to be essential. The excitation of the fine structure levels by the collisions with H atoms is important if $T > 5\,10^3$ K. The same with H_2 molecules is also insignificant in the considered range of density and temperature values (Groenewegen 1993). The cooling due to the excitation of forbidden and resonance lines is effective only if $T \gtrsim 8\,10^3$ K.

The gas temperature $T^{\rm clump}$ has been calculated from Eq. (A1). For the sake of simplicity, each clump was described by a single value of the temperature calculated at its center. It is found that the values of $T^{\rm clump}$ mainly depend on the gas to dust ratio and the distance between the clump and the star. Other clump parameters do not influence the gas temperature. For the gas to dust ratio from 0.1 to 10 of its standard value (see Table 3) and the value of $R^{\rm clump}$ from 3 AU to 50 AU, the temperature was found to be in the range from 200 K to 1000 K.

Note that in the model of Sorelli et al. (1996) $T^{\rm clump} \approx$ 5000 K if a clump is at the distance ~ 0.1 AU from the star.

Appendix B: photoionization rate

The photoionization rate of an atom or ion X of the ground state is

$$\Gamma_{\rm X} = \int_{\nu_{\rm ph}}^{\infty} \sigma_\nu^{\rm X} \, \frac{4\pi J_\nu}{h\nu} \, d\nu. \qquad \text{(B1)}$$

The photoionization cross-sections are approximated as

$$\sigma_\nu^{\rm X} \approx \sigma_0 \left[\frac{a}{x^{\rm s}} + \frac{b}{x^{\rm s+1}} + \frac{c}{x^{\rm s+2}} \right], \qquad \text{(B2)}$$

where σ_0, a, b, c, s are constants and $x = h\nu/I_{\rm p}$. The values of the constants were obtained by least square fitting of the experimental data or the results of theoretical calculations. They are presented in Table 6 (see also Golovatyj et al. 1991). The accuracy of the approximation given by Eq. (B2) is of about 10 – 20%.

For Fe ions, we used the approximation for the cross-sections from Verner et al. (1993).

Appendix C: recombination rates

The rate of radiative recombination $\alpha_{\rm X^+}^{\rm rr}$ is the sum of the recombination rates for all levels of an atom or ion. It is usually represented in the following form

$$\alpha_{\rm X^+}^{\rm rr} = A_{\rm X^+}^{\rm rr} \left(\frac{T_{\rm e}}{10^4\,{\rm K}} \right)^{-\gamma_{\rm X^+}}. \qquad \text{(B1)}$$

The values of constants $A_{\rm X^+}^{\rm rr}$ and $\gamma_{\rm X^+}$ were taken from Golovatyj et al. (1991) or calculated by us.

For ions of C, Mg, Al and Si, the rates of dielectronic recombination $\alpha_{\rm X^+}^{\rm dr}$ have been published by Nussbaumer & Storey (1984, 1986, 1987). The rates for Na and Ca ions are not yet available (Nussbaumer 1992). However, a consideration of the structure of their autoionization levels shows that the rôle of dielectronic recombination should be unimportant provided $T_{\rm e} \leq 8000$ K.

Appendix E: equivalent width of spectral lines

The equivalent width of an absorption line can be calculated if the local density of the atom (or ion) is known at any point in the line of sight. As the source function vanishes in the shell, the equivalent width is (see, e.g., Spitzer 1978)

$$W = \int_{-\infty}^{\infty} \left[1 - \frac{I_\nu}{I_\nu(0)} \right] d\lambda = \frac{\lambda^2}{c} \int_{-\infty}^{\infty} [1 - \exp(-\tau_\nu)] d\nu, \qquad \text{(E1)}$$

where $I_\nu(0)$ is the intensity at the inner boundary of the shell ($R = R_{\rm HII}$).

In general case, the observed absorption line is the superposition of the lines that originate in the shell and clump. Its optical thickness is

$$\tau_\nu = \tau_\nu^{\rm shell} + \tau_\nu^{\rm clump} = \int_{R_{\rm HII}}^{\infty} k_\nu^{\rm shell} \, n_{\rm X^+}(R) \, dR + \\ + \int_{-L_{\rm clump}/2}^{L_{\rm clump}/2} k_\nu^{\rm clump} \, n_{\rm X^+}(r) \, dr, \qquad \text{(E2)}$$

where k_ν is the line absorption coefficient, $n_{\rm X^+}$ number density of the atoms (or ions) at the ground level.

We assumed that both in the shell and the clump the line absorption coefficient has the Doppler profile

$$k_\nu = k_0 \, \exp \left[- \left(\frac{\nu - \nu_0'}{\Delta\nu_{\rm D}} \right)^2 \right]. \qquad \text{(E3)}$$

Here $\nu_0' = \nu_0 \, (1 + v/c)$, ν_0 is the line central frequency in the rest frame, v is equal to the terminal velocity of the wind v_∞ and the projection of the clump orbital velocity on the line of sight $v_r^{\rm clump}$ for the shell and the clump, respectively.

The absorption coefficient at the line center k_0 is connected with the oscillator strength $f_{\rm JJ'}$ (see Table 2)

$$k_0 = \frac{\sqrt{\pi}\, e^2}{m_e c \Delta\nu_{\rm D}} \, f_{\rm JJ'}. \qquad \text{(E4)}$$

Table 6. Constants for the approximation of photoionization cross-sections

Ion	σ_0 (10^{-18} cm^2)	a	b	c	s
H I [(a)]	6.30	1.34	–0.34	0.0	2.99
He I [(a)]	7.83	1.66	–0.66	0.0	2.05
He II [(a)]	1.58	1.34	–0.34	0.0	2.99
C I [(a)]	12.2	3.32	–2.32	0.0	2.0
Na I [(b)]	1.56	1.0	–2.55	1.62	1.35
Mg I [(c)]	1.2	3.0	–2.00	0.0	14
Al I [(d)]	28.2	0.049	–0.529	1.48	2.05
Si I [(d)]	39.2	4.42	0.094	–3.51	2.05
S I [(e)]	12.6	21.6	–40.1	19.5	2.05
Ca I [(f)]	14.4	1.00	0.0	0.0	4.0
Ca II [(g)]	0.1	6.68	–3.24	–1.35	1.50

[(a)] Osterbrock (1974)
[(b)] this work using the data of Weisheit (1972), Yeh & Lindau (1985), Verner et al. (1993)
[(c)] Ditchburn & Marr (1953)
[(d)] Chapman & Henry (1972)
[(e)] Chapman & Henry (1971)
[(f)] this work using the data of Scott et al. (1983)
[(g)] this work using the data of Black et al. (1972)

The Doppler half-width $\Delta\nu_{\rm D}$ is determined by the velocities of gas motions

$$\Delta\nu_{\rm D} = \frac{\nu_0'}{c}\sqrt{v_{\rm th}^2 + v_{\rm turb}^2}, \qquad \text{(E5)}$$

where $v_{\rm th}$ and $v_{\rm turb}$ are the velocities of thermal and microturbulent motions, respectively.

Appendix F: emission coefficient of a hydrogen plasma

The emission coefficient of a hydrogen-like ion with a charge Z was evaluated using the expressions from Sarmiento & Canto (1985)

$$\varepsilon_\nu = Z^2\,\mathscr{K}_0\,\beta_1^{1/2}\,\exp\left(-\frac{h\nu}{kT_{\rm e}}\right)\,\left[g_\nu^{\rm ff}(T_{\rm e}) + f(\nu, T_{\rm e})\right], \qquad \text{(F1)}$$

where

$$\mathscr{K}_0 = \frac{1}{4\,\pi}\,\frac{32\,e^4\,h}{3\,m_{\rm e}^2\,c^3}\,\left(\frac{\pi}{3}\right)^{1/2} = 2.3732\,10^{-41}\,{\rm erg\,cm^{-3}\,s^{-1}}, \qquad \text{(F2)}$$

$\beta_n = Z^2 Ry/n^2/k\,T_{\rm e}$ [$\beta_1 = Z^2\,(157893\,{\rm K}/T_{\rm e})$], $Ry = 13.56$ eV, $g_\nu^{\rm ff}(T_{\rm e})$ is the Gaunt factor for free-free transitions. The function $f(\nu, T)$ can be written as

$$f(\nu, T) = 2\,\beta_1\,\sum_{n=\tilde{m}}^{\infty} n^{-3}\,\exp(\beta_n)\,g_n(\nu). \qquad \text{(F3)}$$

Here, $g_n(\nu)$ is the Gaunt factor for free-bound transitions to the level n. The lower limit $\tilde{m}$ has to be determined from the condition $I_{\tilde{m}-1} \le h\nu \le I_{\tilde{m}}$.

Detailed calculations of the Gaunt factor $g_\nu^{\rm ff}(T_{\rm e})$ have been performed by Carson (1988). Analytical approximations of $g_\nu^{\rm ff}(T_{\rm e})$ are known only for $h\nu/k\,T_{\rm e} \ll 1$ (see, e.g., Kaplan & Pikel'ner 1979). We approximated the results of Carson (1988) in a wide range of the frequency and temperature values as follows ($x = h\nu/I_{\rm p}$)

$$g_\nu^{\rm ff}(T_{\rm e}) \approx \frac{0.446 - 0.551\,\ln(x) + 1.3\,\sqrt{x} + \beta_1\,(1+\sqrt{\beta_1})\,x}{1 + x + \beta_1\,(1+\sqrt{\beta_1})\,x}. \qquad \text{(F4)}$$

References

Berrilli F., Corciulo G., Ingrosso G., et al. 1992, ApJ 398, 254
Black J.H., Weisheit J.C., Laviana E., 1972, ApJ 177, 567
Blondel P.F.C., Tjin A Djie H.R.E., Thé P.S. 1989, A&AS 80, 115
de Boer K.S., Jura M.A., Shull J.M., 1987, in: Scientific Accomplishments of the IUE, ed. Y. Kondo, (Reidel, Dordrecht), p. 485
Böhm T., Catala C., 1995, A&A 301, 155
Cameron A.J.W., 1982, in: Nuclear Astrophysics, eds. C.A. Barnes et al., (Cambridge Univ. Press, Cambridge), p. 23
Carson T.R., 1988, A&A 189, 319
Catala C., 1994, in: The Nature and Evolutionary Status of Herbig Ae/Be Stars, eds. P.S. Thé et al., (ASP Conference Series V. 62), p. 91
Catala C., 1996, private communication
Catala C., Kunasz P.B., 1987, A&A 174, 158 (CK)
Catala C., Kunasz P.B., Praderie F., 1984, A&A 134, 402
Catala C., Czarny J., Felenbok P., Praderie F., 1986a, A&A 154, 103
Catala C., Felenbok P., Czarny J., et al. 1986b, ApJ 308, 791
Catala C., Böhm T., Donati J.-F., Semel M., 1993, A&A 278, 187
Chapman R.D., Henry R.J.W., 1971, ApJ 168, 165
Chapman R.D., Henry R.J.W., 1972, ApJ 173, 243
Ditchburn R., Marr G., 1953, Proc. Phys. Soc., 66, 655
Draine B.T., 1978, ApJS, 36, 595
Dyck H.M., Milkey R.W., 1972, PASP 84, 597
Finkenzeller U., Mundt R., 1984, A&AS 55, 109
Friedemann C., Reimann H.-G., Gürtler J., 1994, Ap&SS 212, 221
Friedemann C., Gürtler J., Reimann H.-G., 1995, A&A 300, 269
Golovatyj V.V., Sapar A.A., Feklistova T.Kh., Kholtygin A.F., 1991, Atomic Data for the Spectroscopy of Rarefied Astrophysical Plasma. Acad. of Science of Estonia, Tallinn
Grachev S.I., 1996, A&A 306, 527
Grinin V.P., 1988, Pis'ma AZh 14, 65
Grinin V.P., Thé P.S., de Winter D., et al. 1994, A&A 292, 165
Grinin V.P., Kozlova O.V., Thé P.S., Rostopchina A.N., 1996, A&A 309, 474
Groenewegen M.A.T., 1993, Ph. D. Thesis, Amsterdam University
Il'in V.B., Krivov A.V., 1994, in: The Nature and Evolutionary Status of Herbig Ae/Be Stars, eds. P.S. Thé et al., (ASP Conference Series V. 62), p. 177
Il'in V.B., Voshchinnikov N.V., 1993, Astron. Rep. 37, 362
Kaplan S.A., Pikel'ner S.B., 1979, Physics of Interstellar Medium. Nauka, Moscow
Kholtygin A.F., 1995, in: Proc. 4th Workshop on Multi-site Continuous Spectroscopy, eds. L. Huang et al., (ESA/ESTEC), p. 299
Krivova N.A., Il'in V.B., 1996, in: The Role of Dust in the Formation of Stars, eds. H.U. Käufl, R. Siebenmorgen, (Springer), p. 187
Kurucz R.L., 1979, ApJS 40, 1
Mitskevitch A.S., 1995, A&A 298, 231
Morton D.C., 1991, ApJS 77, 119
Nishi R., Nakano T., Umebayashi T., 1991, ApJ 368, 181
Nussbaumer H., 1992, private communication
Nussbaumer H., Storey P.J., 1984, A&AS 56, 293
Nussbaumer H., Storey P.J., 1986, A&AS 64, 545
Nussbaumer H., Storey P.J., 1987, A&AS 69, 123
Osterbrock D.E., 1974, Astrophysics of Gaseous Nebulae. Freeman, San Francisco
Praderie F., Talavera A., Felenbok P., et al. 1982, ApJ 254, 658
Prusti T., Mitskevitch A.S., 1994, in: The Nature and Evolutionary Status of Herbig Ae/Be Stars, eds. P.S. Thé et al., (ASP Conference Series V. 62), p. 257
Roy A.E., 1978, Orbital Motion. Adam Hilger, Bristol
Rudzikas Z.B., Nikitin A.A., Kholtygin A.F., 1991, Theoretical Atomic Spectroscopy. Leningrad University Press, Leningrad
Sarmiento A., Canto J., 1985, Rev. Mex. Astron. Astrofis. 11, 61
Scott P., Kingston A.E., Hibbert A., 1983, J. Phys. B16, 3945
Skinner S.L., Brown A., Stewart R.T., 1993, ApJS 87, 217
Sorelli C., Grinin V.P., Natta A., 1996, A&A 309, 155
Spitzer L., 1978, Physical Processes in the Interstellar Medium. Wiley, New York
Spitzer L., Jenkins E.B., 1975, ARA&A 13, 133
Striganov A.R., Odintsova G.A., 1982, Tables of spectral lines of atoms and ions. Energoizdat, Moscow
Thé P.S., de Winter D., Pérez M.R., 1994, A&AS 104, 315
Tielens A.G.G.M., Hollenbach D., 1985, ApJ 291, 722
Timoshenko L.V., 1985, Afz 22, 51
Timoshenko L.V., Filip'ev G.K., 1983, Afz 19, 513
Tjin A Djie H.R.E., Thé P.S., Andersen J., et al. 1989, A&AS 78, 1

Turner B.E., 1991, ApJ 376, 573
Verner D.A., Yakovlev D.G., Band I.M., Trzhakovskaya M.B., 1993, Atomic Data Nucl. Data Tables 55, 233
Voshchinnikov N.V., Grinin V.P., 1992, Afz 34, 84
Voshchinnikov N.V., Grinin V.P., Kiselev N.N., Minikulov N.Kh., 1988, Afz 28, 182
Voshchinnikov N.V., Grinin V.P., Karjukin V.V., 1995, A&A 294, 547
Voshchinnikov N.V., Molster F.J., Thé P.S., 1996, A&A 312, 243
Weisheit J.C., 1972, Phys. Rev. A5, 1621
Wenzel W., 1969, in: Non-Periodic Phenomena in Variable Stars, ed. L. Detre, (Proc. IAU Coll. N 42, Budapest), p. 61
Wenzel W., Dorschner J., Friedemann C., 1971, Astron. Nachr. 292, 221
de Winter D., 1996, Ph. D. Thesis, Amsterdam University
Yeh J.I., Lindau I., 1985, Atomic Data Nucl. Data Tables 32, 1

This article was processed by the author using Springer-Verlag LaTeX A&A style file *L-AA* version 3.